Tail-Based Anchoring on Granular Media for Transporting Heavy Payloads

Joshua Fernandez and Anirban Mazumdar

***Abstract*—Granular media, like sand, restricts vehicle traction and degrades the ability of mobile robots to pull loads. Solutions that are effective on hard or clean surfaces fail on sand. This work presents a mobile robot system that utilizes an active tail to greatly increase its ability to pull loads. The robot combines dynamic tail impacts, plowing, and leveraging of cable tension to achieve this improved performance. The key contributions of this letter are 1) illustrating how dynamic impacts can provide substantial anchoring force on two terrain types, 2) incorporating anchoring behavior into tail actuator design, 3) combining tail and wheel behaviors to create granular barriers, 4) leveraging geometry to utilize winch tension for enhanced performance, and 5) experimentally demonstrating the ability to transport loads 6x the robot mass on a deep sandy surface. The prototype 7.6 kg robot was able to pull a 45.5 kg load on a deep sand surface. This is a substantial improvement over the baseline robot which was only able to pull a 13.6 kg load.**

***Index Terms*—Mechanism Design, Robotics in Hazardous Fields, Engineering for Robotic Systems.**

I. Introduction

UTILIZING mobile robots to transport large payloads can help improve industrial productivity, logistics, search and rescue, and even space exploration. If robots can pull several times their weight, they can provide unique capabilities and may even exceed the capacities of humans. To this end, there have been many innovations in transport of relatively heavy items which include using gecko-inspired adhesives on smooth surfaces [1], robots with spines on rough surfaces [2], and legged robots on paved asphalt [3].

However, granular media such as sand or regolith present different challenges for payload transport. Specifically, achieving sufficient friction or anchoring on sandy surface remains difficult. Gecko-inspired adhesives do not perform well on dirty surfaces since they rely on surface-level interactions, and microspines perform poorly on sand [4], [5]. Similarly, legged robots have shown degraded performance on sand [6].

There have been recent innovations in designing robots for sand terrain [7]–[9]. However, these works have focused on locomotion, not payload transport. For payload transport, we seek the ability to anchor the robot to the ground, and then use a winch to drag a load. The robot then releases the anchor and can move again. This process can be repeated to move loads over long distances.

Fig. 1. A photograph of a robot system designed to pull loads on granular media.

This methodology is similar to prior approaches and does not require the robot to lift or carry the load. However, this approach requires sufficient ground friction to bear the tensile loads from the winch. Current robots cannot achieve sufficient friction on sand to transport loads that are substantially heavier than the robots themselves.

To solve this challenging problem, we draw inspiration from how animals use their tails to anchor to the environment. Nature is filled with several such examples, including monkeys and seahorses [10], [11]. Similarly, we utilize a mobile robot's tail to create anchoring behaviors in sand. Our work differs from previous works on robotic tails which have primarily focused on self righting and agility [12]–[15]. As we show in Fig. 1, we equip a custom-designed rover with a unique tail mechanism and a winch. The tail features a high-torque electromagnetic actuator coupled to small $(2:1)$ gear reduction. Dynamic impact force is maximized by the tail end-effector burying deep into the sand. This differs from previous studies of dynamic impacts and actuation [16]. The robot's wheels can be coordinated with the tail burial to plow the granular media. This creates greater anchoring forces by creating a wall. Finally, the winch cable is also routed so that the rope tension increases tail performance. This combination of behaviors enables the robot to pull payloads that have 6x more mass (45.5 kg) than the robot (7.6 kg).

The key contributions of this letter are 1) illustrating how dynamic impacts can provide substantial anchoring force on two terrain types, 2) incorporating anchoring behavior into tail actuator design, 3) combining tail and wheel behaviors to create granular barriers, 4) leveraging geometry to utilize winch tension for enhanced performance, and 5) experimentally demonstrating

Manuscript received October 6, 2020; accepted January 22, 2021. Date of publication February 4, 2021; date of current version February 17, 2021. This letter was recommended for publication by Associate Editor Prof. Gianluca Palli and Edito Prof. Clement Gosselin upon evaluation of the reviewers' comments. *(Corresponding author: Joshua Fernandez.)*

The authors are with the G. W. Woodruff School of Mechanical Engineering, Georgia Institute of Technology, Atlanta, GA 30332 USA (e-mail: jfernandez75@gatech.edu; anirban.mazumdar@me.gatech.edu).

This article has supplementary downloadablematerial available at https://doi.org/10.1109/LRA.2021.3057289, provided by the authors.

Digital Object Identifier 10.1109/LRA.2021.3057289

the ability to transport loads 6x the robot mass on a deep sandy surface.

II. Design Overview

This work seeks to enable wheeled mobile robots to transport relatively large loads over granular and other soft media. We pursue a similar architecture to previous works [4] that use a mobile robot and a motorized winch to gradually transport a payload. Our robot uses a tail with a single plate at its end to insert into the ground and resist horizontal movement. The single plate design was chosen to reduce weight and possible interference between parallel plates.

To enhance the current-state-of-the-art, a wheeled mobile robot should be able to pull loads that are substantially greater than the robot mass on granular and soft terrain. We define this metric as the "payload transport ratio" which is computed by dividing the payload mass by the mobile robot mass. Since such robot-level performance has not been previously measured on such terrain, there are no existing benchmarks. The simplest method for enhancing the payload transport ratio is to reduce the payload friction. Our studies have shown that using a smooth box with a wheeled robot provides a payload ratio of $2.1:1$. This work seeks to substantially exceed this performance.

In addition, the mobile robot should also be capable of reversible anchoring. This is needed to maintain robot mobility and enable payload transportation over long distances. Finally the mobile robot design should have the capacity to autonomously attach/detach from the payload. Our investigations of the existing literature showed that there are no current systems that can meet both the aforementioned requirements.

In the following sections we outline our three core enabling principles that provide enhanced performance. These principles are dynamic tail impacts, plowing granular media, and intelligent routing of winch cable. We follow this section with a description of our prototype mobile robot that integrates the three enabling principles. This prototype design uses manual attachment, but we illustrate how the tail can be used to create a range of autonomous attachment devices. We conclude with a discussion of our experimental results.

III. Principle 1: Dynamic Tail Impacts

Our work focuses on utilizing a robotic tail to enable anchoring in the sand. We insert the tail into the sand in order to increase friction/anchoring. The tail has a flat plate that is driven into the sand in order to create an anchoring or resistive force. The resistive force, F_r, can be computed using known relationships for granular media:

$$F_r = \gamma g \rho w x_i^2 \tag{1}$$

where γ is the dimensionless constant (grain surface/morphology/packing), g is the gravitational constant, ρ is the density of the granular media, w is the width of the plate, and x_i is the insertion depth [17].

From this equation we can see that the only design parameters are the width of the plate and the depth of insertion. Width is limited by the size of the robot. Insertion depth is more flexible, and increases with depth squared. Therefore, we focus on maximizing depth. We examined two methods for maximizing depth of insertion: static insertion and dynamic impact.

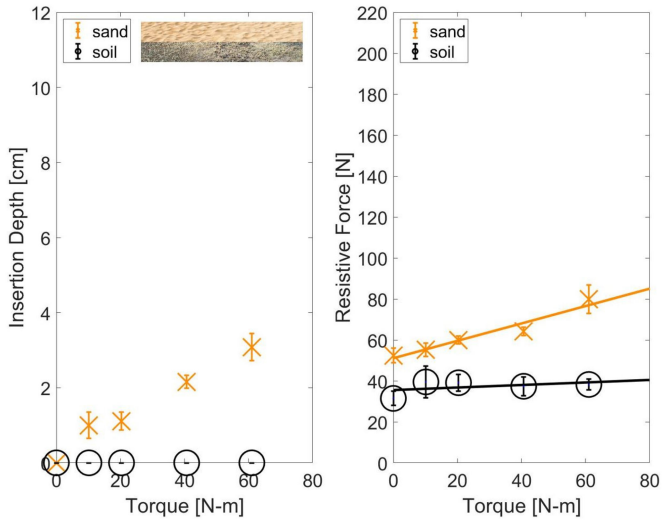

Fig. 2. Experimental data showing insertion depth (a) and resistive force (b) achieved using static insertion methods on sand and soil.

A. Static Insertion Experiments

The static method uses the motor to slowly and continuously push the tail into the sand until the torque is too large for the motor to overcome. This method is well aligned with heavily geared-servo motors that can produce relatively large torques but cannot move quickly.

To simulate the performance of static torque, a robust tail (1.4 kg) was attached to the sand rover (6.8 kg) and weights of varying amounts were placed on the tip of the tail (w = 30.5 cm). The weights used were 2.25, 4.5, 9, 13.5, and 18 kg. The torque necessary to provide this weight at the end of the tail can be calculated using the tail length (45.7 cm). Once the weight was placed on the tail, the tail sunk into the granular media. After it finished sinking, we recorded the insertion depth. We then removed the external load from the tail. Next, a force scale applied a horizontal load on the tail. The peak load produced by the force scale before tail movement was recorded as the peak resistive force. We performed ten independent trials for each weight. Two separate terrains were examined: sand and soil. The insertion depth and the resistive force are illustrated in Fig. 2.

B. Dynamic Impact Experiments

Dynamic impacts offer an alternative method of insertion. Impacts can leverage kinetic energy and momentum to create very large transient forces. This can be achieved by using small gear ratios and high-torque motors [18]. Dynamic impacts offer promise because insertion does not require sustained forces/torques.

We simulated dynamic impacts by dropping weights from various heights onto the tail. The test heights ranged from

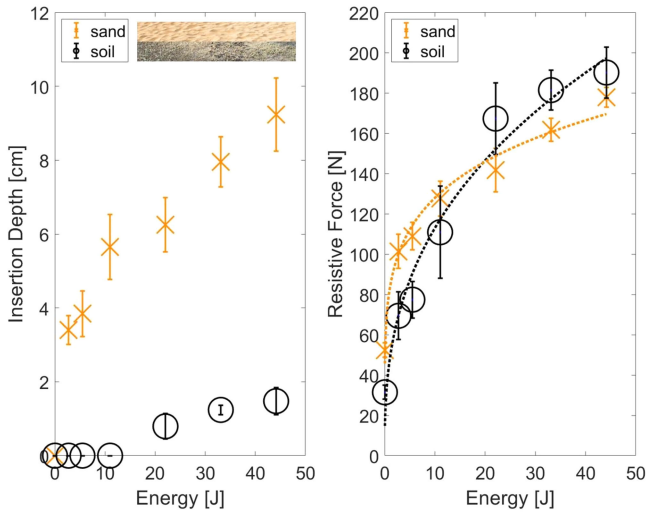

Fig. 3. Experimental data showing insertion depth (a) and resistive force (b) achieved using dynamic insertion methods on sand and soil.

0.063 m–1 m. The impact energy was determined by the gravitational potential energy. The external weight was then removed. The insertion depth and resistive force were measured after each impact. We performed ten independent trials for each height on both sand and soil. The results of this experiment can be seen in Fig. 3.

To model the ground-tail interaction, we fit the experimental resistive force data to curves. Using the static insertion method, the fit was linear. Using the dynamic impact method, the fit followed a power curve. These are shown in Figs. 2 and 3. The curves can be used to predict the resistive force for various designs as long as they operate in the vicinity of the experimental data point.

Since dynamic impacts use energy while static methods use torque, it is difficult to compare them directly with only experimental data. However, the experimental results do show interesting differences between sand and soil. In soil, static methods perform more poorly in terms of both insertion depth and force. Dynamic methods provide improved insertion depth in soil, but the resistive force is similar to sand. These results illustrate that the media type must be carefully characterized early in the design process.

C. Analytical Models

The experimental results can be combined with actuator models to examine tradeoffs between static and dynamic methods. These methods can also be used to inform tail actuator design.

We created a simple electro-mechanical model of the tail and impact dynamics. We assumed that the tail starts from rest and only travels 180° before impacting the sand. Expressions are provided in Eqs. (2)–(5). Numerical forward simulation was used to compute the final velocity and impact energy of the tail. The final kinetic energy can be easily computed using the mass of the tail (m_t) and the tail endpoint velocity (v_t).

$$\tau_m = \frac{(V_{in} - k_e \dot{\theta} N) k_t}{R} \tag{2}$$

$$\frac{d\dot{\theta}}{dt} = \frac{\tau_m N - T_L(\theta, m_t)}{J_m N^2 + I_L} \tag{3}$$

$$v_t = L\dot{\theta} \tag{4}$$

$$E = \frac{1}{2} m_t v_t^2 \tag{5}$$

Equation 2 calculates the output torque of the motor shaft by subtracting the the back emf ($k_e\dot{\theta}$) times the gear ratio (N) from input voltage (V_{in}). Then that quantity is multiplied by the torque constant (k_t) and divided by the internal resistance of the motor (R). In 3, angular acceleration is determined using the motor torque (τ_m), torque of the load ($T_L(\theta, m_t)$), the inertia of the motor ($J_m N^2$), and inertia of the load (I_L). The velocity of the tail endpoint, v_t, can be computed using the length of the tail, L. L is the critical tail length of 45.7 cm which is determined by the analysis in Section V. Lastly, the kinetic energy of the tail is given by 5.

Static force due to motor torque can be computed more easily. To find the torque of the output shaft, the peak torque of the motor is multiplied by the gear ratio. Then, the static force that pushes into the sand is found by dividing the output torque by the tail length.

D. Comparing Static and Dynamic Insertion

The data-driven curves for resistive force can be used to predict the resistive forces from both static and dynamic insertion methods. For static insertion we assume the motor provides a short torque at it's maximum momentary torque value. For dynamic insertion we assume the motor provides maximum voltage in order to achieve the greatest impact energy. The static torque increases linearly with motor gearing, but impact energy is a more complex function.

To provide a comparison between static and dynamic methods, we used a single candidate motor (Maxon EC 90 flat Ø90 mm 600 W) and predicted both static and dynamic resistive force for a range of gear ratios. For these studies, the length and mass of the tail were held fixed. The results for both sand and soil are shown in Fig. 4, and are normalized by the weight of the tail and rover. Using dynamic impact, The results illustrate that modest gear ratios can achieve high resistive forces. It would take substantial gear ratios to exceed this performance statically. Such gear ratios would add substantial mass and complexity. Therefore, the remainder of this work will utilize dynamic tail impacts.

E. Actuator Design for Dynamic Insertion

Now that we have selected dynamic impacts as our method for insertion into granular media, we need to choose the best parameters. In theory, the free design parameters are the gear ratio and the tail mass. In practice, the gear ratio may be restricted by packaging, fabrication, and integration constraints.

Using the experimental curve fits for impact in sand and the electro-mechanical model of the tail, we can anticipate the achieved resistive force for a given gear ratio and tail mass. First, we sweep over gear ratios (1–25) and tail masses (0–2.5 kg) and

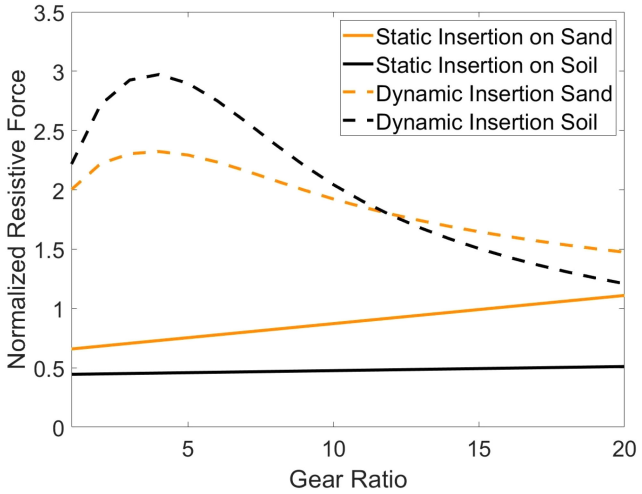

Fig. 4. Simulated data showing the normalized resistive force as a function of gear ratio .

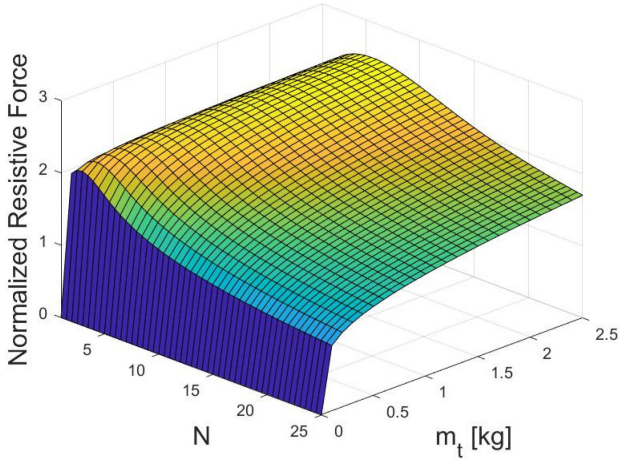

Fig. 5. Simulated data showing the normalized resistive force as a function of gear ratio and tail mass.

generate impact energies using the electro-mechanical model. Then, we use the experimental curve fit in order to project the resistive force for a given impact energy. Fig. 5 shows the results normalized by the experimental tail and rover mass.

The results illustrate some important trends. First, for each tail mass, there is an optimal gear ratio. This ratio is relatively modest due to the need for rapid speeds and accelerations. The optimal normalized resistive force on the plot is 2.5075 and is located at a gear ratio of $N = 5.5$ and a tail mass of $m_t = 2.5\,\mathrm{kg}$. The normalized resistive force is still slowly increasing gradually beyond 2.5 kg, but it is unlikely that the extra mass is worth the marginal benefit.

The results of our analysis can be utilized by tail designers based on their unique actuation and size requirements. For our case, we chose to utilize $N = 2$ and $m_t = 0.8\,\mathrm{kg}$. We chose these because a $2:1$ gearbox is more compact and a 0.8 kg tail balances strength and weight. These parameters result in a normalized resistive force of 2.2208, which is close to the optimal configuration.

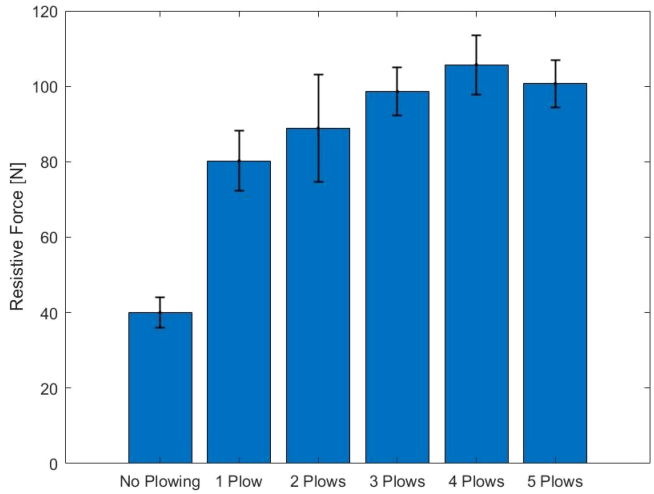

Fig. 6. Experimental data showing resistive force as number of plows is increased.

IV. Principle 2: Plowing

Plowing is another effective strategy for increasing the overall resistive force from the tail. Specifically, the wheels of the robot can be used to create a wall of sand behind the tail. During plowing, the tail is dropped to the surface of the granular media and is used as a plow to move the granules. In granular media, each granule interacts with one another through particle-particle interaction. These interactions consist of normal and shear forces that each granule exerts on one another [19]. Therefore, by increasing the number of granules behind the tail, the resistive force can potentially be increased.

In order to examine plowing in our system, we used our wheeled robot to plow the sand. Specifically, we examined how the number of plow cycles influenced the resistive force. In this experiment, the rover dropped its tail to the surface of the sand. Then it drove backward which allowed the tail to plow the sand into a wall. The rover can then drive forward and repeat this process again to create a taller and more dense wall. In our experiment, the rover's resistance to horizontal load was evaluated for 0–5 plows. Six experiments were performed for each plow cycle.

The results are shown in Fig. 6. This figure illustrates that plowing can substantially increase the resistive force of the robot-plus-tail system. The greatest increase in resistive force comes between no plowing and a single plow. In this case, the resistive force doubles (40 N to 80 N). With each successive plow, the resistive force increases slightly and reaches its peak between 3 and 5 plows.

V. Principle 3: Exploiting Winch Tension

The third principle is utilizing the winch tension to increase resistive force. The winch cable is under tension when pulling the payload. If this tension can be used to push the tail into the sand, then greater anchoring can be achieved. Fig. 7 illustrates how the winch cable can be routed to increase the downward force.

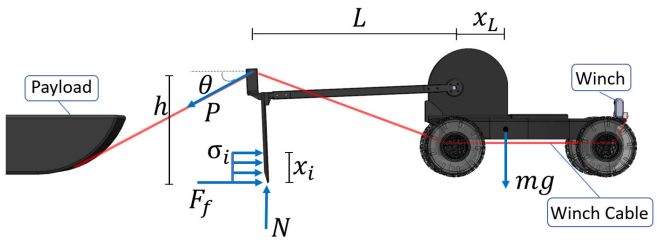

Fig. 7. A free body diagram for static stability analysis.

Specifically, we created a tail design that directs the winch tension downward on the tail. This means that as the winch starts pulling on the payload, a portion of the tensile force, P, pushes the tail into the sand. As seen in Fig. 7, the winch is located at the front of the robot. The winch cable (denoted in red) is routed under the body and to the top of the tail using a pulley system. From the top of the tail, the winch cable is attached to the payload.

While this cable routing can improve anchoring, the moment around the tip of the tail that it creates can cause the rover to flip over. Flipping over can degrade performance and may prevent the robot from recovering its mobility. Therefore, we need to determine geometric parameters that prevent flipping under the expected loads.

From the force diagram depicted in Fig. 7, we can use static analysis to analyze our system at the moment flipping occurs. In this force diagram, we describe our system as the rover and the tail. The forces acting on the system are the force of the payload at the top of the tail (P), the friction force (F_f), the normal force of the tail and wheels on the ground (N), the the resistive force stemming from insertion as a force per unit length (σ_i), and the force of gravity (mg). In Fig. 7, the normal force is located at the tail tip because when flipping occurs, all four wheels of the rover come off the ground. Once the tail is properly inserted into the sand and payload pulling begins, the winch tension causes the tail to physically contact the bumper of the rover. These contact forces are internal forces and do not affect the flipping of our system.

$$\sum F_x = 0 = \sigma_i x_i + F_f - Pcos(\theta) \tag{6}$$

$$\sum F_y = 0 = N - mg - Psin(\theta) \tag{7}$$

$$\sum M = 0 = -mg(L + x_L) + Pcos(\theta)h - \sigma_i \frac{x_i^2}{2} \tag{8}$$

The static force balance for the x and y directions are provided in 6 and 7. The key equation is the sum of the moments. We sum the moments at the location where the equivalent point normal force would be applied. As mention previously, we assume a worst case scenario where the equivalent normal force is located at the end of the tail. It should be noted it would only be located this far to the rear of the vehicle as flipping is occurring. This assumption provides conservative results and enables simplified analysis.

$$Pcos(\theta) = \sigma_i x_i + F_f \tag{9}$$

$$N = mg + Psin(\theta) \tag{10}$$

$$L_s = \frac{Pcos(\theta)h - \sigma_i x_i^2/2}{mg} - x_L \tag{11}$$

The expressions can be used to calculate the critical length for the tail that ensures stability, L_s. The expression for L_s is provided in 11. For our specific example, we computed the critical tail length, L_s, early in the design process in order to optimize impacts and size all the parts. We utilized L_s as our tail length, L.

Friction and insertion depth were determined with preliminary experiments. We wanted the robot to be able to pull a 68 kg load along the sand. We assumed a coefficient of friction between the payload and the sand of $\sim$0.3. The resistive force per length, σ_i, was calculated from the impact tests and was estimated to be 0.24 N/m. Note that the cable angle, θ depends on the distance between the robot and the payload. The angle increases as the payload is pulled closer, and the tipping margin is reduced. The cable angle can be managed by controlling the rovers proximity to the payload and we chose to use $\theta = 15^\circ$ because it roughly matched our upper bound during experiments. The insertion depth, x_i, was estimated to be 7.6 cm based on our previous experiments. The mass of the rover, m, was assumed to be 6.8 kg. This is slightly lower than the final mass of the vehicle, but it also provides a conservative result. Based on these numbers, we computed a critical tail length, L_s of 45.7 cm. The tail length throughout this letter assumes this value.

VI. Physical Prototype

A custom prototype was designed and assembled around the three core enabling principles. The following sub-section describes the prototype which consists of a custom sand rover, the novel tail system, and the electronics.

A. Sand Rover

Our system is based around a four-wheel-drive rover. Each wheel is driven by a geared DC motor (Servo City #638 280). The tires have a diameter of 12.3 cm, and feature rubber treads for improved traction. The rover body is 3D printed and reinforced with aluminum brackets. The rover body is 38.1 cm long and 27.9 cm wide.

For payload transport, we incorporated a 1/10 Warn 8274 winch into the front of the rover. The rover pulls with a fishing line rated for 454 N. The fishing line is fed through a three-pulley system based on the cable routing described in Section V. A photograph of the rover (without the tail) is shown in Fig. 8.

B. Tail Design

The tail was made of an aluminum I-beam and attached to a 30.5 cm x 15.2 cm x 0.6 cm plastic plate. A 3-D printed pulley is mounted to the top of the plastic plate. The tail is 45.7 cm long, and is powered by a Maxon EC 90 flat Ø90 mm 600 W brushless motor. The motor is coupled to a 2 : 1 spur gear reduction. The tail mass is 0.8 kg and is concentrated near the end of the tail. The tail design can be seen in Fig. 9. The tail is projected to generate an impact energy of 57.5 J.

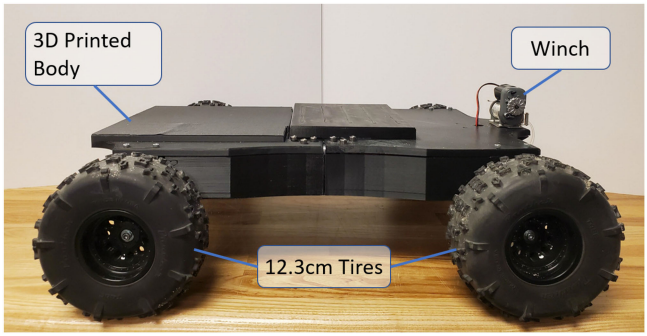

Fig. 8. A photograph of the sand rover platform.

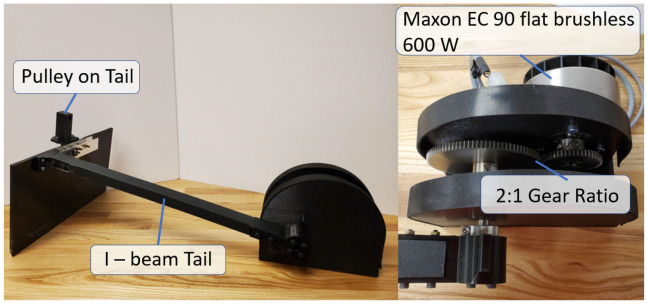

Fig. 9. Images illustrating the tail design (a) and the actuation (b).

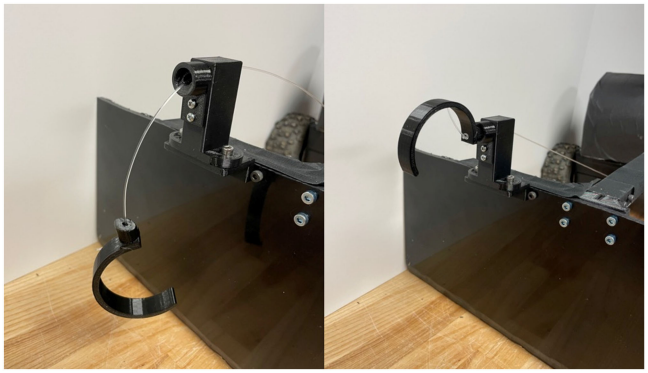

Fig. 10. The hook payload attachment mechanism on the tail.

The tail is designed in a way that allows for different payload attachment mechanisms. In our design, a payload attachment mechanism can be affixed to the winch cable which is fed through a 3-D printed pulley at the top of the tail. When the cable is pulled taunt so that the attachment mechanism is flush against the pulley, our attachment mechanism is designed so that it will always be at the same position and orientation. Maintaining this position and orientation can be achieved by designing the payload attachment mechanism and pulley so that they have complementary geometries. We do this by designing the end of the pulley and mechanism to have triangular features that slide into each other when they make contact (Fig. 10). This allows for the hook design as seen in Fig. 10 to always be parallel to the ground and facing downward. This type of passive attachment requires coordination between the tail and the rover.

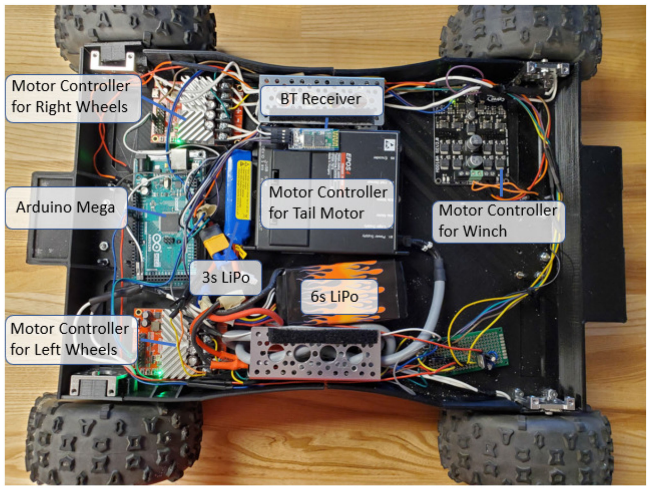

Fig. 11. A photograph of the electronics in the sand rover.

The rigid tail also provides a range of options for actively controlling the hook. For example, a servo motor can be attached to the tail near the hook to engage or disengage spring-loaded features. Similarly, actuators can be added to the hook and used to engage electrical contacts on the tail. The actuator would only be used when the hook is fully retracted. However, the wires would not need to be spooled with the winch.

Both the active and passive payload attachment mechanisms will allow for the rover to back into a payload and latch onto it. Since the payload attachment mechanism can be tailored to the payload, this enables the rover to attach and detach to any target payload. For simplicity in our experiments, our gripper was a simple U design that was attached to the payload by a human teammate prior to the experiments.

C. Electronics

The rover motor drivers, batteries, mircontroller, and communication modules are all enclosed within the rover body. An Arduino MEGA microcontroller is used to generate commands to the wheels, the winch, and the tail. The wheels are driven by a pair of Roboclaw 2×30 A brushed motor drivers. The winch is driven by a Cytron Dual Channel 10 A DC motor driver. The tail motor is driven by a Maxon EPOS4 70/15 brushless motor controller. The wheels and winch are powered by a 3 cell (11.1 V) LiPo battery. The tail motor is powered by a 6 cell (22.2 V) LiPo battery.

For the scope of this work, the robot is primarily controlled using human manual control. The human operator sends commands to the Arduino MEGA via a HC-06 Bluetooth module. The electronics are shown in Fig. 11. The fully assembled robot prototype has a mass of 7.6 kg. Without the tail system, the robot has a mass of 4.4 kg.

VII. Performance

Outdoor testing was performed at a sand pit at the Georgia Institute of Technology. A series of experiments were performed to quantify the performance of our overall system and its various subcomponents.

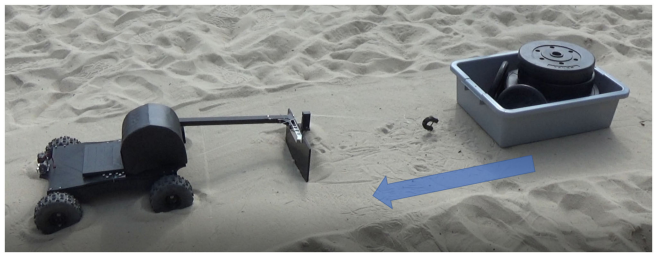

Fig. 12. A photograph illustrating the payload pulling tests with a standard tub.

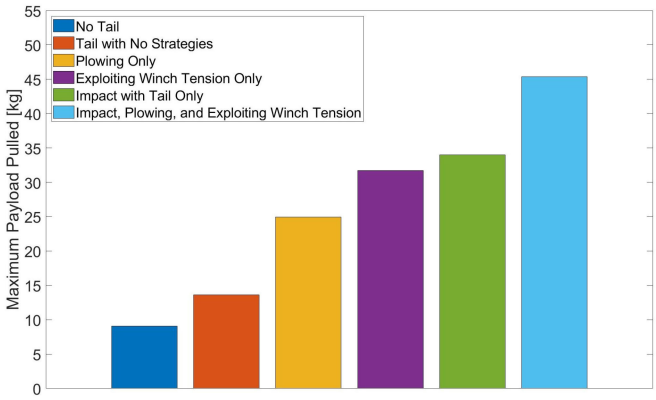

Fig. 13. Experimental data showing the payload transport capacity with various enabling principles.

Our tests consisted of measuring the payload mass quantity that the rover could pull using the winch before the wheels began to slip. For consistency, the sand was smoothed, and the payload was placed in a rectangular plastic tub. Maximum payload testing was conducted by placing a known weight in the bin and then having the winch pull the payload. If the prototype succeeded in pulling the payload, 5 lbs. was added to the bin and the prototype attempted to move the payload again. This was done until the payload caused the sand anchor to fail. For this and subsequent tests, failure was defined as the robot rover displacing a full body length. A photo of an experimental system is shown in Fig. 12.

We performed 6 experiments, each with 3 trials. We started by pulling a load with no tail attached to the prototype. Then, we performed a baseline that used the full rover but its tail remained in the stowed position. Third, the tail was used to plow before pulling. Fourth, we employed the exploiting winch tension strategy. Fifth, we used the dynamic impact strategy. Lastly, we employed all three strategies to determine the maximum payload of the system.

The averaged experimental results are illustrated in Fig. 13. These illustrate the progressive improvement over the baseline rover. The rover without the added mass of the tail was only able to pull 9 kg. Given the robot mass of 4.4 kg, this represents a payload transport ratio of $2.1:1$ With the additional mass of the tail, the rover pulled 13.6 kg. Given the robot plus tail mass of 7.6 kg, this represents a payload transport ratio of $1.8:1$. Note how simply adding mass does not improve the payload transport ratio. This trial was considered the "baseline" because for equal comparison the weight of the tail (although not used) must be included. Then the individual strategies where tested. Plowing alone enables the rover to increase its payload ability to 25 kg, exploiting winch tension enables the rover to pull 31.75 kg, and dynamic tail impact enables the rover to pull 34 kg. Finally, incorporating all the strategies enables payload transport up to 45.5 kg. The three core principles in this work combined to increase payload capacity on sand by $3.3x$. The full prototype robot has a mass of 7.6 kg. Therefore, the payload transport ratio is $6:1$. Although our principles increase resistive force with the ground, they do not eliminate mobility. The robot is able to dislodge its tail from the ground, release tension in the winch, and then continue moving.

Our experiments illustrated that a rectangular container is not well suited for long distance transport because a pile of sand eventually forms in front of it. This increases the required pulling force. This requires addressing the payload rather than the robot. We incorporated a snow sled and repeated the baseline and 3-principle experiments with this sled. These experiments are illustrated in the accompanying video, and demonstrate that a common sled enables better pay-load transport. The overall performance with the sled is similar to the initial container with the combined principles pulling 45.5 kg. The advantage of the sled is that it prevents sand build up and can therefore be pulled over much longer distances.

VIII. Conclusion

This letter presents a novel anchoring system for transporting heavy payloads across granular media. We compared static torque and dynamic impact and determined that dynamic impact increased insertion depth. We then developed a model of the system to determine how the mass properties, gear ratio, and length of the tail influence impact energy and resistive force. Also, we showed that using the tail as a plow allowed for a sand wall to develop and increase resistive force. Additionally we showed that by leveraging winch tension, we could further increase load capacity.

Finally, we combined all three core principles into a prototype mobile robot. The unique sand rover prototype was able to pull a payload that was $6x$ its own mass. The payload capacity was improved by $3.3x$. These results were achieved without compromising the mobility of the rover. The rover is capable of removing its tail from the ground and driving further.

In addition to demonstrating new experimental results, this letter provides data and analysis that can be generalized by designers and applied to a range of applications and size scales. We are optimistic that these methods will enable robots to increase their performance in challenging granular environments.

Acknowledgment

The authors would like to thank J. Donoghue and C. Donoghue for their help in prototyping and testing during the COVID-19 quarantine. They would also like to thank the Accessibility, Rehabilitation, and Movement Science (ARMS) NSF Traineeship Program (Award Number: 1 545 287) for their support and funding.

REFERENCES

[1] D. L. Christensen, E. W. Hawkes, S. A. Suresh, K. Ladenheim, and M. R. Cutkosky, "μtugs: Enabling microrobots to deliver macro forces with controllable adhesives," in *Proc. IEEE Int. Conf. Robot. Automat.*, 2015, pp. 4048–4055.

[2] A. Parness, N. Abcouwer, C. Fuller, N. Wiltsie, J. Nash, and B. Kennedy, "Lemur 3: A. limbed climbing robot for extreme terrain mobility in space," in *Proc. IEEE Int. Conf. Robot. Automat.*, 2017, pp. 5467–5473.

[3] M. Hutter *et al.*, "Anymal-a highly mobile and dynamic quadrupedal robot," in *Proc. IEEE/RSJ Int. Conf. Intell. Robots Syst.*, 2016, pp. 38–44.

[4] Geckos May Be Famously Sticky, but Here's What Stumps Them," Jul. 2016, Library Catalog: Www.nationalgeographic.com Section: News. Accessed: Aug. 10, 2020. [Online]. Available: https://www.nationalgeographic.com/news/2016/07/animals-science-geckos-reptiles-sticky/

[5] A. Parness *et al.*, "Gravity-independent rock-climbing robot and a sample acquisition tool with microspine grippers," *J. Field Robot.*, vol. 30, no. 6, pp. 897–915, 2013.

[6] S. Komizunai, A. Konno, S. Abiko, X. Jiang, and M. Uchiyama, "Dynamic simulation of biped walking on loose soil," *Int. J. Humanoid Robot.*, vol. 09, pp. 1–20, Jan. 2013.

[7] C. Li, P. B. Umbanhowar, H. Komsuoglu, D. E. Koditschek, and D. I. Goldman, "Sensitive dependence of the motion of a legged robot on granular media," *Proc. Nat. Acad. Sci.*, vol. 106, no. 9, pp. 3029–3034, 2009.

[8] B. Liu, Y. Ozkan-Aydin, D. I. Goldman, and F. L. Hammond, "Kirigami skin improves soft earthworm robot anchoring and locomotion under cohesive soil," in *Proc. 2nd IEEE Int. Conf. Soft Robot.*, 2019, pp. 828–833.

[9] H. Marvi *et al.*, "Sidewinding with minimal slip: Snake and robot ascent of sandy slopes," *Science*, vol. 346, no. 6206, pp. 224–229, 2014.

[10] P. Lemelin, "Comparative and functional myology of the prehensile tail in new world monkeys," *J. Morphol.*, vol. 224, no. 3, pp. 351–368, 1995.

[11] R. Nuwer, "Why Seahorses Have Square Tails," Library Catalog: Www.smithsonianmag.com Section: Articles, Science, Wildlife, Accessed: Aug. 10, 2020. [Online]. Available: https://www.smithsonianmag.com/science-nature/why-seahorses-have-square-tails-180955802/

[12] W. Saab, W. S. Rone, A. Kumar, and P. Ben-Tzvi, "Design and integration of a novel spatial articulated robotic tail," *IEEE/ASME Trans. Mechatronics*, vol. 24, no. 2, pp. 434–446, Apr. 2019.

[13] Y. Liu and P. Ben-Tzvi, "Design, Analysis, and integration of a new two-degree-of-freedom articulated multi-link robotic tail mechanism," *J. Mechanisms Robot.*, vol. 12, no. 2, Apr. 2020, publisher: American Society of Mechanical Engineers Digital Collection. [Online]. Available: https://asmedigitalcollection.asme.org/mechanismsrobotics/article/12/2/021101/1072243/Design-Analysis-and-Integration-of-a-New-Two

[14] C. S. Casarez and R. S. Fearing, "Dynamic terrestrial self-righting with a minimal tail," in *Proc. IEEE/RSJ Int. Conf. Intell. Robots Syst.*, Sep. 2017, pp. 314–321.

[15] R. Briggs, J. Lee, M. Haberland, and S. Kim, "Tails in biomimetic design: Analysis, simulation, and experiment," in *Proc. IEEE/RSJ Int. Conf. Intell. Robots Syst.*, Oct. 2012, pp. 1473–1480.

[16] P. M. Wensing, A. Wang, S. Seok, D. Otten, J. Lang, and S. Kim, "Proprioceptive actuator design in the mit cheetah: Impact mitigation and high-bandwidth physical interaction for dynamic legged robots," *IEEE Trans. Robot.*, vol. 33, no. 3, pp. 509–522, Jun. 2017.

[17] R. Albert, M. Pfeifer, A.-L. Barabási, and P. Schiffer, "Slow drag in a granular medium," *Phys. Rev. Lett.*, vol. 82, no. 1, pp. 205–208, 1999.

[18] A. Wang, J. Ramos, J. Mayo, W. Ubellacker, J. Cheung, and S. Kim, "The hermes humanoid system: A. platform for full-body teleoperation with balance feedback," in *Proc. IEEE-RAS 15th Int. Conf. Humanoid Robots*, 2015, pp. 730–737.

[19] N. Gravish, P. B. Umbanhowar, and D. I. Goldman, "Force and flow at the onset of drag in plowed granular media," *Phys. Rev. E*, vol. 89, no. 4, 2014. Art. no. 042202.